Eur. Phys. J. A **12**, 15–28 (2001)

THE EUROPEAN PHYSICAL JOURNAL A

Study of ^{169}Hf at high rotational frequency

K.A. Schmidt[1], M. Bergström[1], G.B. Hagemann[1,a], B. Herskind[1], G. Sletten[1], P.G. Varmette[1], J. Domscheit[2], H. Hübel[2], S.W. Ødegård[3], S. Frattini[4], A. Bracco[4], B. Million[4], M.P. Carpenter[5], R.V.F. Janssens[5], T.L. Khoo[5], T. Lauritsen[5], C.J. Lister[5], S. Siem[5], I. Wiedenhöver[5], D.J. Hartley[6], L.L. Riedinger[6], A. Maj[7], W.C. Ma[8], and R. Terry[8]

[1] The Niels Bohr Institute, Blegdamsvej 17, DK-2100 Copenhagen Ø, Denmark
[2] Institut für Strahlen- und Kernphysik, University of Bonn, Nussallee 14-16, D-53115, Bonn, Germany
[3] Department of Physics, University of Oslo, Norway
[4] Dipartimento di Fisica, University of Milano and INFN Milano, Italy
[5] Argonne National Laboratory, Argonne, Illinois 60439, USA
[6] Department of Physics and Astronomy, University of Tennessee, Knoxville, TN 37996, USA
[7] Niewodniczanski Institute of Nuclear Physics, Krakov, Poland
[8] Mississippi State University, Mississippi State, MS 39762, USA

Received: 23 March 2001 / Revised version: 20 September 2001
Communicated by D. Schwalm

Abstract. High-spin properties of the nucleus ^{169}Hf have been studied through the fusion evaporation reaction ^{96}Zr(^{76}Ge,3n)^{169}Hf at a beam energy of 310 MeV. The known rotational bands have been extended considerably and 6 new bands have been established, four of which form coupled bands with pronounced $M1$ connections. Quasiparticle assignments are suggested for the new band structures, and it appears that coupling to vibrational degrees of freedom plays a role. Both coupled bands involve the excitation of quasiprotons. In the region of highest spin, a large alignment gain is interpreted in terms of a mixed crossing where an $h_{9/2}$ and an $h_{11/2}$ quasiproton provide the two signatures of the aligning configuration.

PACS. 21.10.-k Properties of nuclei; nuclear energy levels – 23.20.Lv Gamma transitions and level energies – 25.70.-z Low and intermediate energy heavy-ion reactions – 27.70.+q $150 \leq A \leq 189$

1 Introduction

Cranked shell model calculations with the code Ultimate Cranker [1,2] gave rise to hopes that triaxially superdeformed (TSD) states would become yrast at attainable spins in the hafnium nuclei ($Z = 72$). With this motivation in mind experiments with the Gammasphere [3] and Euroball [4] γ-detector arrays were proposed to probe the high-spin region of the hafnium nuclei. As a result of the Gammasphere experiment, TSD bands were indeed discovered by automatic search routines in the main reaction product ^{168}Hf [5]. Unfortunately, a similar approach in ^{169}Hf yielded negative results.

The most recent high-spin spectroscopic study of ^{169}Hf by Gao *et al.* [6] reports two pairs of bands built on the lowest positive- and negative-parity orbitals, $[642]5/2^+$ and $[523]5/2^-$, respectively. Lifetime measurements [6] confirmed the deformation expected from cranking calculations for both orbitals.

Although the present study did not lead to the discovery of TSD bands in ^{169}Hf, several other interesting features were revealed. In the case of new rotational bands, it is our goal to determine the associated quasiparticle configuration, aided by measured and calculated DCO ratios, $B(M1)/B(E2)$ ratios, neighbouring nuclei systematics as well as by comparison to Ultimate Cranker calculations. One and three-quasiparticle configurations are dominant in this even-odd nucleus, but for a few bands extended to the high-spin region, five quasiparticle configurations will be considered as well. In this spin region, proton excitations are expected and a section of this paper is devoted to a discussion of the candidate proton pairs.

The experiment is outlined below in sect. 2, followed by a presentation of the main results in sect. 3, including spin and parity assignments of the new bands. Section 4 contains a more detailed discussion of the configuration assignments as well as the nature of observed high-frequency crossings.

[a] e-mail: hagemann@nbi.dk

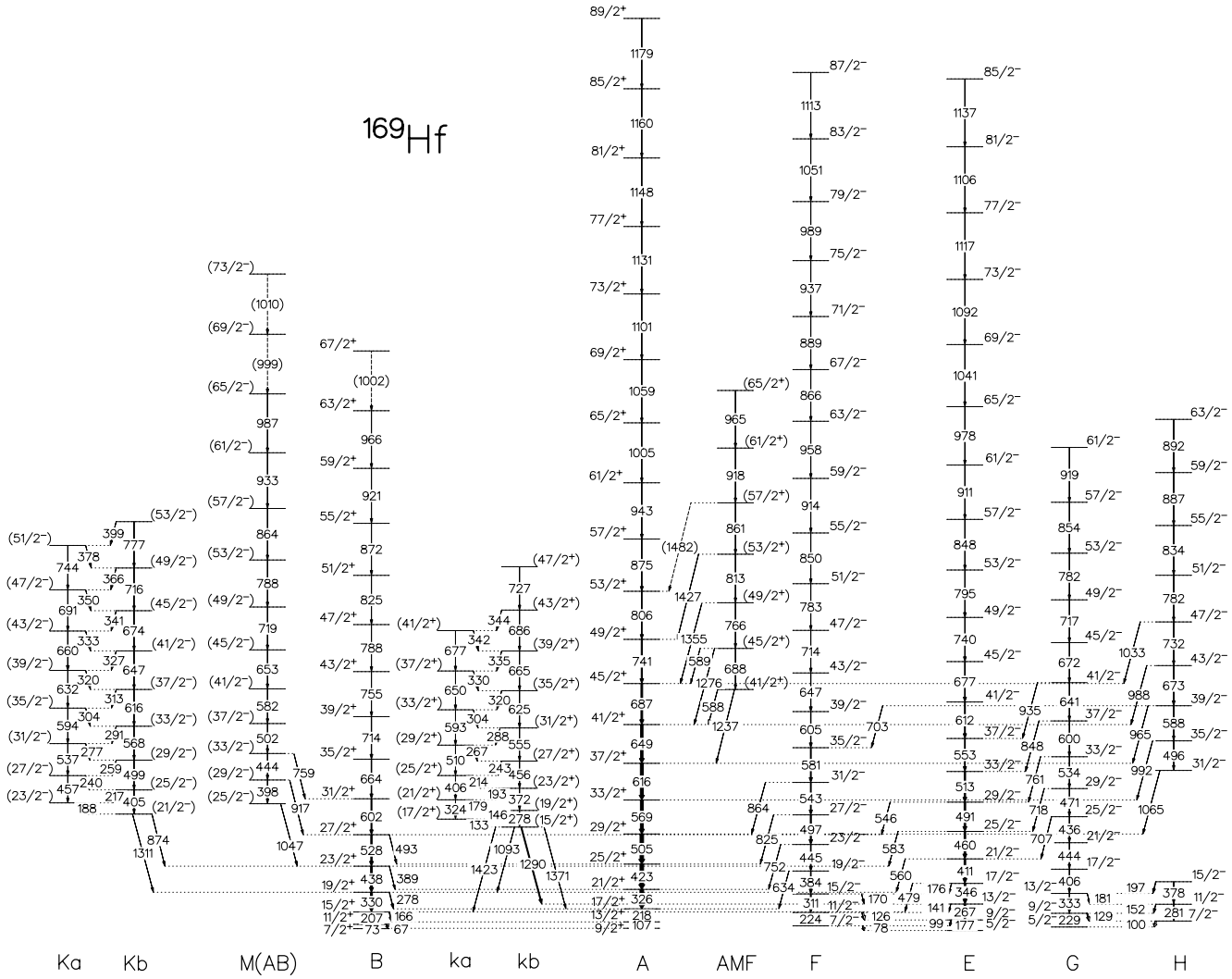

Fig. 1. The level scheme of ^{169}Hf based on previous [6,9,10] and present work. The bands are labeled according to their configuration using the cranking model notation (see table 1). Possible configurations for the new strongly coupled bands Ka,Kb and ka,kb are discussed in the text.

2 Experimental technique

The high-spin states of the odd-neutron nucleus ^{169}Hf were populated in a cold, near-symmetric fusion reaction involving large angular momentum. Targets of ^{96}Zr, ranging in thickness from 600 μg/cm^2 to 700 μg/cm^2 and enriched to 85.25%, were bombarded by a 310 MeV ^{76}Ge beam provided by the ATLAS accelerator at the Argonne National Laboratory. The dominant reaction channels include evaporation of three, four and five neutrons, while the charged-particle channels were found to be about ten times weaker.

The Gammasphere array [3], equipped with 101 single HPGe detectors, each with a Compton suppression shield and a BGO backplug, collected γ-ray coincidence data. The online gain matching of the detectors was applied and a total of $2.2 \cdot 10^9$ events of fivefold or higher was collected.

The high-fold data were broken down and sorted into several symmetrized cubes of γ-γ-γ coincidence data and symmetrized hypercubes of γ-γ-γ-γ coincidences. Additionally, an isolation of the high-spin data of the 3n and 4n channels was sought, by setting a 2D gate on the total γ-energy (H) as a function of the coincidence fold (k). The level scheme analysis was completed with the LEVIT8R and 4DG8R programs from the Radware package [7]. Information about the multipolarity of the transitions was obtained from the analysis of DCO ratios. For this purpose, the high-fold data was sorted into an asymmetric cube where the energies measured in the foward and backward detectors were stored along the x-axis, the energies measured at 90° were stored on the y-axis and the z-axis was used to store the information of all the detectors. By gating on the z-axis, matrices suitable to extract the DCO ratios were generated and the analysis was completed with the XMii program [8]. Strong transitions of known multi-

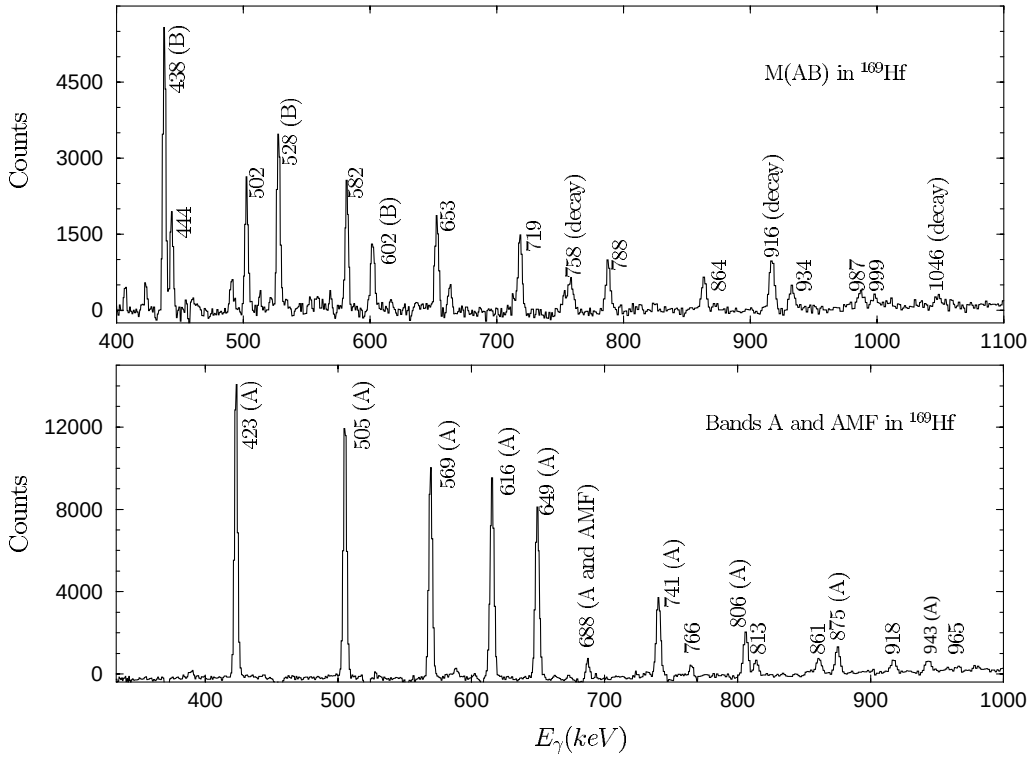

Fig. 2. Sample coincidence spectra illustrating the quality of the data. Top: spectrum of the M(AB) band, from a sum of double coincidence gates consisting of the 330 keV transition in band B and a gate list containing the transitions of band M(AB). Three transitions of band B are seen as are the three decay transitions feeding band B. Bottom: a weak band is revealed at the foot of the intense band A. The spectrum is a sum of double gates consisting of a gate list of the transitions in band AMF and the 326 keV transition of band A.

polarity were used to calibrate the DCO ratios. When the gating transition was a stretched $E2$ transition, the DCO ratio was found to have an average value of 0.98 ± 0.04 for a γ-ray of stretched $E2$ character, while the ratio had a value of 1.57 ± 0.10 for a stretched dipole ($E1$) transition.

3 Results

The established level scheme, including previous studies [6,9,10], is shown in fig. 1. Labels are explained in table 1. Four of the highest-spin transitions in the level scheme of ref. [6] have been altered as our analysis points to a different scenario. Energies of the new levels and γ-rays are listed in table 6 (see Appendix A.). All new bands have suggested spin assignments from DCO ratios and, in a few cases, from population intensities. Spins are assigned under the assumption that stretched quadrupole transitions are of $E2$ nature and stretched dipole transitions of $E1$ rather than $M1$ nature. Stretched $M1$ transitions in the range of 0.5–1.5 MeV would usually be mixed with unstretched $E2$ transitions, which compete due to the E_γ^5 strength factor. The coincidence relationships documenting the new and extended band structures are shown in figs. 2 and 3.

Table 1. Relevant neutron orbitals, quasiparticle labels and experimental alignment as observed in the present experiment.

ν orbitals	Alignment i_X
$[651]3/2^+$ C, D	
$[642]5/2^+$ A, B	4.0, 3.0
$[523]5/2^-$ E, F	1.5, 1.5
$[512]5/2^-$ G, H	0.0, 0.0
$[521]1/2^-$ M, N	2.5

3.1 Band crossings in known bands

As is customary, the rotational bands of this nucleus are labelled according to table 1, which includes the most relevant orbitals as determined from Nilsson diagrams. The use of parentheses indicates the alignment of a pair of quasiparticles.

The assignments are taken from ref. [9]. The Nilsson orbital associated with bands G and H is chosen in accordance with measured (g_K-g_R)-values [9]. The $[521]3/2^-$ orbital is expected lower in excitation energy, but in the neighbouring ^{167}Hf the two orbitals, $[512]5/2^-$ and $[521]3/2^-$, are both present and mix [11]. Our bands G and H could be associated with either of those possibilities at higher spins.

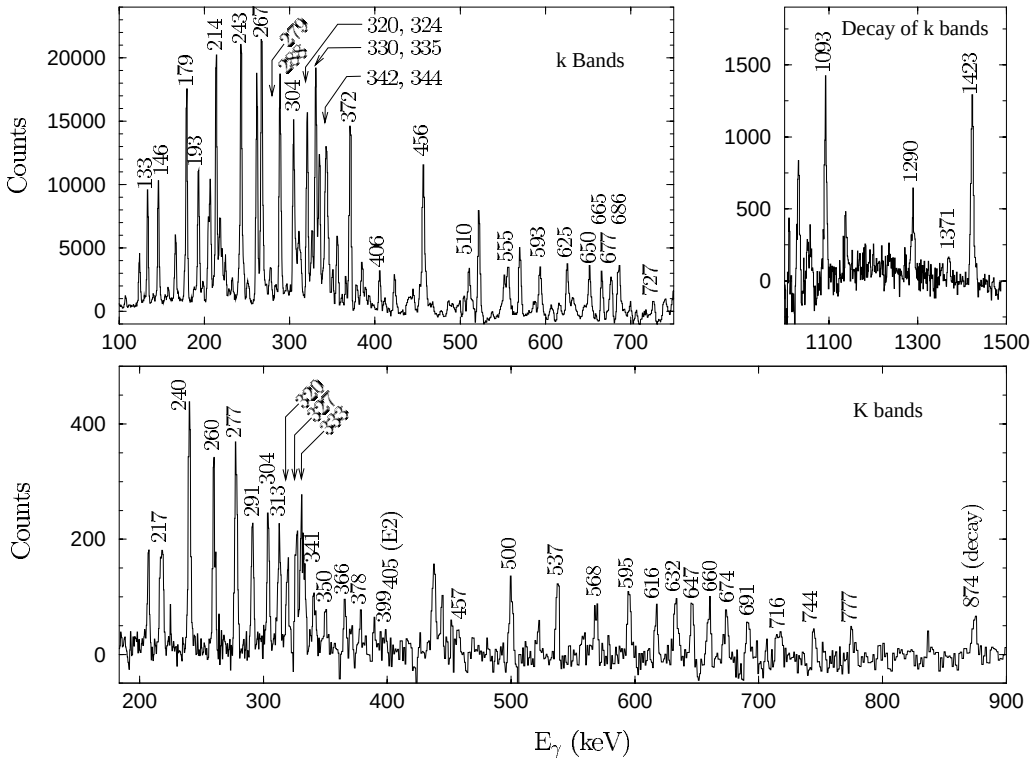

Fig. 3. Top: spectrum of the bands ka and kb, produced using a sum of double gates of a gate list containing the $M1$ transitions of the k bands. The low-energy, high-intensity transitions are of $M1$ character while the mid-energy, low-intensity transitions are of $E2$ multipolarity. Two observed decays to band B (1093 and 1423 keV) and single decays to band A (1371 keV) and band E (1290 keV) are presented in the top right panel. Bottom: double coincidence gate on the 188 keV and 217 keV transitions. As above, the low-energy, high-intensity transitions have $M1$ multipolarity, while their mid-energy counterparts are $E2$'s. The strong 874 keV decay to band B is evident.

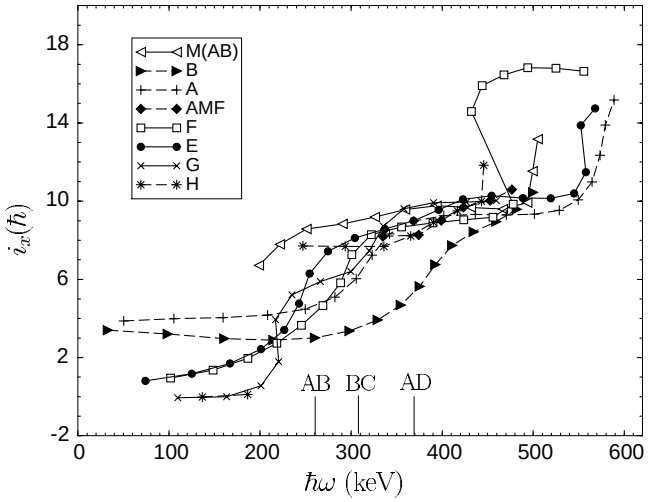

Fig. 4. Alignment of all bands, except bands ka,kb, Ka and Kb, relative to a reference with Harris parameters $\mathcal{J}_0 = 35\hbar^2\,\mathrm{MeV}^{-1}$ and $\mathcal{J}_1 = 40\hbar^4\,\mathrm{MeV}^{-3}$. The AB, BC and AD band crossings are marked (see subsect. 3.1 for details).

The six previously known bands of ^{169}Hf, A, B, E, F, G and H, were considerably extended, revealing one, and in some cases, two band crossings.

A note should be made about the eight new levels believed to belong to the H band. They appear to be the extension to higher spins of this band as can be seen on an E *vs.* I plot (see fig. 11, below) and the levels have the correct spin and parity. However, three intermediate levels are missing in band H, most likely due to the intense decay out to band A, a pattern quite common for such bands [12]. Band H is seen to interact with band F at $I \sim 35/2$–$39/2$, causing the presence of a 703 keV $39/2^-(H) \rightarrow 35/2^-(F)$ transition. This interaction is not surprising as the orbital, associated with the bands G and H, is similar in structure to the orbital associated with the bands E and F. An identical situation has been documented in ^{163}Er [12]. Alternatively, the eight levels forming the high-spin part of band H could be assigned to the negative signature of the $[521]1/2^-$ orbital with the AB quasineutrons aligned, N(AB). One of the new bands is assigned to the partner, M(AB), see subsect. 4.2. The H(AB) and N(AB) configurations could be mixed, and a sharp distinction between the two configurations may not be possible.

The observed crossings, illustrated in fig. 4, are ordered in table 2 according to theoretical expectations, although they occur experimentally at slightly higher frequencies. The tendency towards the prediction of band crossings at lower frequencies than observed, may be explained by

Table 2. Observed and theoretical band crossing frequencies for the first band crossing in bands A, B, E, F, G and H. The theoretical frequencies have been determined from UC calculations, see text for details.

Band	Crossing	$\hbar\omega$ (observed)	$\hbar\omega$ (theory)	$\Delta\hbar\omega$	i_X gain (observed)
E	AB	260 keV	210 keV	+50 keV	$7.5\hbar$
F	AB	270 keV	210 keV	+60 keV	$7.5\hbar$
G	AB	255 keV	210 keV	+45 keV	$8.0\hbar$
H	AB	255 keV	210 keV	+45 keV	$6.5\hbar$
A	BC	310 keV	295 keV	+15 keV	$5.5\hbar$
B	AD	370 keV	325 keV	+45 keV	$6.0\hbar$

the lack of collectiveness of the cranking potential, which leads to an erroneous moment of inertia [13]. The second crossing, at high frequency, experienced by bands A, E, F and M is discussed in subsect. 4.5.

3.2 Spin and parity assignment to new bands

For each of the new bands the spin and parity determination for the various levels were carried out as independently as possible from theory. These spin assignments rely primarily on DCO ratios, but relative population also serves as a guideline.

The first new band (see fig. 2) is labelled M(AB), consistent with our quasiparticle assignment. Three decay transitions of high energy connect band M(AB) to band B. These transitions are presumably stretched dipoles as an E *vs.* I plot indicates that the band should be more intensely populated if they were stretched quadrupoles, in which case the band would become yrast for $I \leq 30.5\hbar$. In the case of unstretched quadrupole transitions one would have expected competing stretched $E2$ decays of higher energy, which have not been observed. The stretched dipole nature is further supported by DCO measurements for the 916 keV decay transition which yield an average ratio of 1.36 ± 0.42 relative to a stretched $E2$ transition in band B or within band M(AB) itself. Transitions of $M1$ character are ruled out on the basis that they are unlikely at such high energies. We suggest that the decay is of stretched $E1$ nature and band M(AB) is assigned negative parity.

The second new band, in fig. 2, is labelled AMF in accordance with its assigned configuration. Seven decay transitions connect this band to the intensely populated band A. An intensity argument reverse to the one given for band M(AB) suggests that these transitions are of $E2$ multipolarity, five of these with $\Delta I = 2$ and the remaining two with $\Delta I = 0$. This places band AMF in the energy vicinity of bands G and H. The credibility of this scenario was tested by setting similar coincidence gates in bands G, H and AMF. Investigated transitions in the three bands were shown to have comparable intensities in a common-spin region. The parity of band AMF is thus positive. The DCO measurements were not able to confirm this picture due to the low statistics of the data, resulting in very large uncertainties.

Figure 3 shows two sets of coupled bands connected by $M1$ transitions that were uncovered in our data set. Bands Ka and Kb are depopulated through two transitions from Kb to band B, while bands ka and kb experience four decays from kb to states of both positive and negative parity. The I^π possibilities are $23/2^+$, $21/2^+$, $21/2^-$ or $19/2^+$for the lowest state of Kb. The 874 keV decay of the band Kb yielded an average of 1.25 ± 0.19 for three DCO measurements of this transition (relative to a stretched $E2$ transition in band B), indicating stretched dipole rather than stretched quadrupole nature, which rules out $19/2^+$. Due to a rather large uncertainty mixed $M1/E2$ multipolarity cannot be excluded. The lower population of Ka,Kb relative to bands G,H and AMF implies that $I^\pi = 23/2^+$, which would bring Ka,Kb as low as band H at $I = 55/2$, is very unlikely. We suggest $I^\pi = 21/2^-$ as the solution most compatible with both intensity and DCO data, although $I^\pi = 21/2^+$ cannot be strictly excluded. The branching ratio of the two decay branches, $T_\gamma 1311$ keV/$T_\gamma 874$ keV ~ 0.2, does not reflect an E_γ^3 relation. Structural effects must also play a role in the $E1$ decay. For the lowest state of kb the I^π possibilities are $17/2^-$ or $15/2^+$. The relative population of the two bands, Ka,Kb and ka,kb, demands a separation on an E *vs.* I plot. DCO measurements were not conclusive in the case of the decay transitions of the band kb. With $I = 21/2$ for the lowest state of Kb it follows from the intensity argument that $15/2^+$ is the preferred spin and parity of the lowest level of the k bands. Furthermore, a spin and parity of $17/2^-$ for this level would place the two bands, presumably then of identical parity, unreasonably close over a long sequence of levels. It is, therefore, suggested that the spin and parity of the lowest level of the bands ka,kb is $15/2^+$.

4 Discussion

4.1 Ultimate Cranker calculations

Cranking calculations for the ^{169}Hf nucleus have been carried out with the Ultimate Cranker [1,2] program. In the normal deformed (ND) region the deformation is predicted to be quite stable. Proton and neutron orbital energies are displayed on the Routhian diagrams of fig. 5, and the orbitals relevant to our level scheme have been labelled. Notice that Nilsson orbitals are indicated in the proton diagram as a quasiparticle labelling scheme has not been

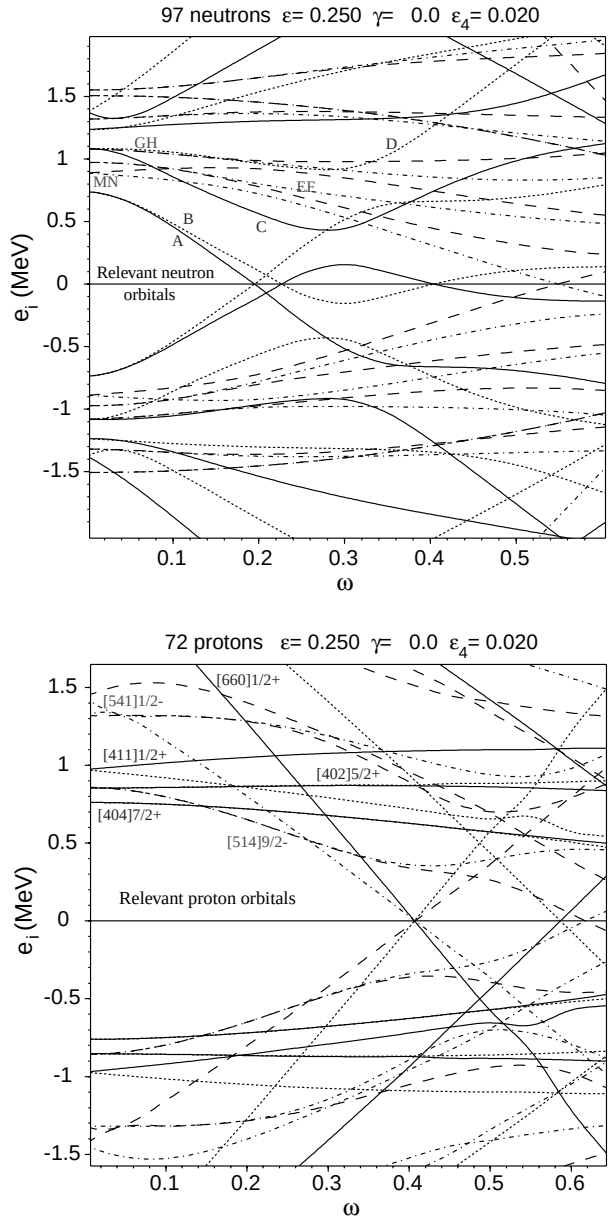

Fig. 5. Routhian diagrams for neutrons (top) and protons (bottom). Full (dotted) lines indicate positive parity and signature +1/2 (positive parity and signature −1/2). Dashed (dashed and dotted) lines indicate negative parity and negative signature (negative parity and positive signature).

defined for protons. It is worth pointing out that several of the neutron orbital energies are dependent on deformation. Most profound is the switching of the EF and MN orbital pairs, *i.e.* the EF orbital becomes lowest in energy for a deformation of $\varepsilon_2 = 0.200$. For $\varepsilon_2 = 0.250$, the MN orbital is placed below the GH orbital, a picture which is not supported by the observed populations of the E, F, G, H, M(AB) and AMF bands. Therefore, we consider the Ultimate Cranker calculation to be slightly erroneous, having placed the MN orbital too low relative to the other orbitals.

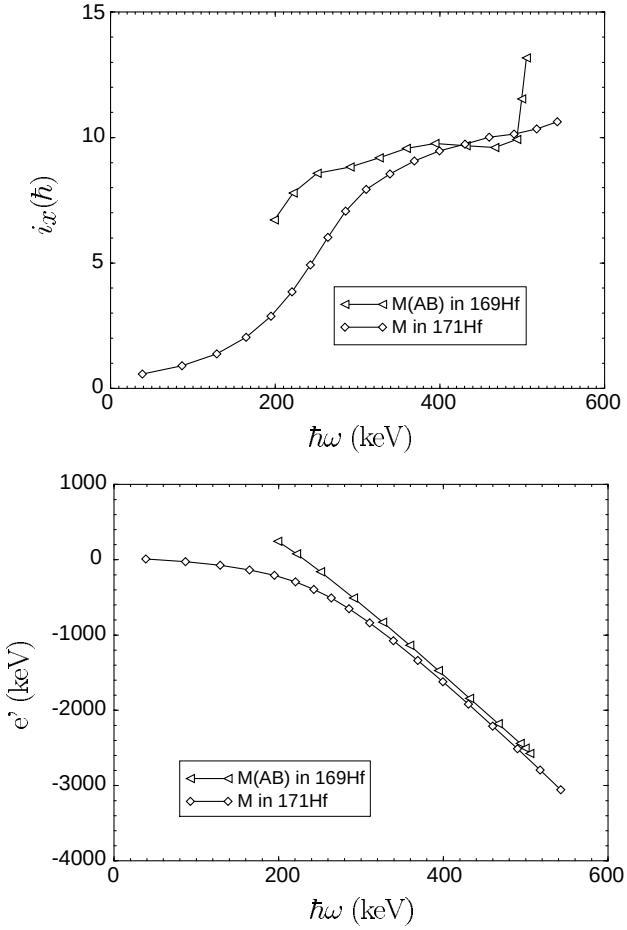

Fig. 6. Top: alignment of band M(AB) in ^{169}Hf and band M in ^{171}Hf, relative to a reference with Harris parameters $\mathcal{J}_0 = 35\hbar^2\,\mathrm{MeV}^{-1}$ and $\mathcal{J}_1 = 40\hbar^4\,\mathrm{MeV}^{-3}$. Bottom: Routhians for the same bands.

4.2 Configuration assignment of band M(AB)

The alignment plot of the negative-parity band M(AB), fig. 6, points to a three-quasiparticle configuration beginning just at the AB crossing. Ultimate Cranker calculations suggest a low-lying, negative-parity orbital with $\Omega = 1/2$. This $[521]1/2^-$ orbital (M), which is found in numerous nuclei in this region, is the prime configuration candidate for band M(AB). The M orbital is the ground state of ^{171}Yb, ^{173}Hf and ^{169}Er and found as an excited state in ^{171}Hf, ^{173}Yb, ^{169}Yb, ^{167}Yb and ^{167}Er. It is also part of an excited multi-quasiparticle state in the nuclei ^{172}Yb, ^{170}Tm and ^{169}Er [10]. In fig. 6, the alignment and Routhian of band M of ^{171}Hf is compared to that of band M(AB). Band M of ^{171}Hf experiences an AB crossing at about $\hbar\omega = 260$ keV. Beyond this frequency, this band and band M(AB) of ^{169}Hf exhibit similar Routhians. Due to a local gap in the neutron single-particle level energy, the interaction strength of the AB crossing has a dominant neutron number dependence around $N = 98$ [14]. The interaction strength is much larger for $N = 99$ than for $N = 97$ and, consequently, the alignment gain is ex-

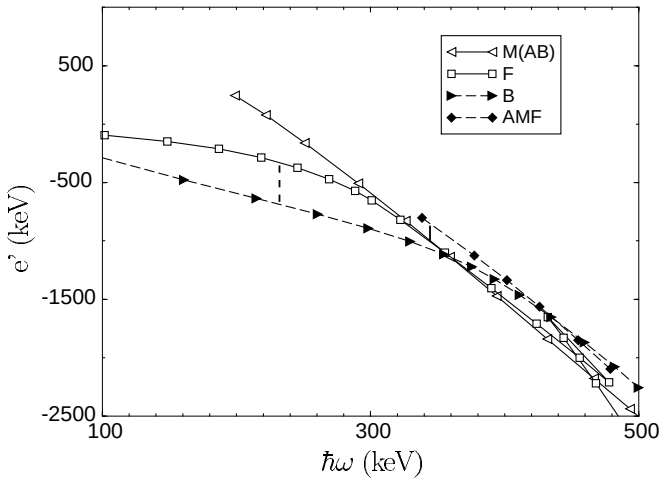

Fig. 7. Routhians for bands B, F, AMF and M(AB) relative to a reference with Harris parameters $\mathcal{J}_0 = 35\hbar^2\,\mathrm{MeV}^{-1}$ and $\mathcal{J}_1 = 40\hbar^4\,\mathrm{MeV}^{-3}$. The difference between bands B and F is indicated by the dashed vertical line, while the difference between bands AMF and M(AB) is marked by the solid vertical line.

pected to be smoother for ^{171}Hf as is indeed the case. The large upbend of band M(AB) at $\hbar\omega = 490$ keV will be discussed in subsect. 4.5. The consistency between the two bands in the region 300 keV$< \hbar\omega <$ 475 keV leaves us confident in our configuration assignment of M(AB) for the band in ^{169}Hf.

4.3 Assignment of band AMF, γ-vibration coupling

Ratios of the $B(E2)$-values for the decay transitions *vs.* the in-band transitions of band AMF were extracted. The average ratio was about 5%, which, with the assumption of a transition quadrupole moment Q_t of the in-band transitions of $\sim$ 6b, in agreement with our UC calculations and ref. [6], corresponds to $B(E2)$ values for the decay transitions of $\sim 0.068\ e^2b^2$ which is of the order of 10 W.u. (omitting the statistical factor). This is substantially higher than expected for $E2$ decays of such high energy, and is in the range of values expected for vibrational transitions, suggesting the possibility of mixing with a γ-vibrational state. The latter is known to enhance the strength of the $E2$ transitions to the band on which the γ-vibration is built. A similar picture of increased branching ratios has been discovered in ^{163}Er [12], where the enhancement of the decay transitions is linked to a γ-vibrational component of the wave function, achieved by a $K = 2$ coupling in the band configuration. Encouragingly, γ-vibrational bands are present in ^{166,168,170}Hf [10], although the $\Delta I = 0$ inter-band transitions of 751 keV and 652 keV for ^{166}Hf and ^{168}Hf, respectively, are slightly higher in energy than the 588 keV transition in ^{169}Hf. This could advocate that the vibrational excitation energy is lower in ^{169}Hf than in its even-even neighbours, but may just as well be due to different moments of inertia as the vibrational state of ^{169}Hf is found at much higher spins. Strongly suspecting a γ-vibrational coupling, a two-quasiparticle configuration with $K = 2$ coupled to A was assigned to band AMF. This allows coupling to the quadrupole degrees of freedom, hereby accounting for the enhanced transition rates. The two-quasiparticle configuration, $[521]1/2^- \downarrow \otimes [523]5/2^- \uparrow$, has $K = 2$ between its components and, when coupled to the A orbital, results in the correct parity and alignment. The suggested configuration is thus AMF mixed with the γ-vibration built on A. Figure 7 shows a lowering in energy of band AMF with respect to band M(AB). The difference between bands B and F ($\approx$ 350 keV) is clearly larger than the difference between bands AMF and M(AB) ($\approx$ 185 keV). The band pairs cannot be compared at exactly the same frequencies. The comparison is made as close in frequency as possible, in regions escaping crossings. The difference between band AMF and band M(AB) outweighs the difference between bands F and B by 150–200 keV. It is our belief that the interaction of band AMF with the γ-vibration causes the observed lowering of the energy.

Table 3. Relevant proton orbitals with associated experimental alignments as determined from neighbouring nuclei [10] and calculated gyromagnetic ratios.

π orbitals	Alignment i_x	Gyromagnetic ratio g_K
$g7/2[404]7/2^+$	0.0	0.63
$h9/2[541]1/2^-$	3.5	0.76
$d3/2[411]1/2^+$	0.0	−0.98
$d5/2[402]5/2^+$	0.0	1.77
$i13/2[660]1/2^+$	4.0	1.22
$h11/2[514]9/2^-$	0.5	1.29

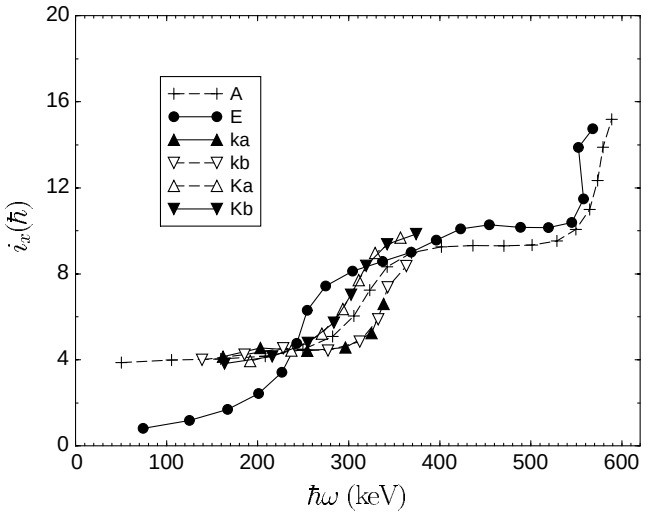

Fig. 8. Alignment of bands A, E, ka,kb and Ka,Kb relative to a reference with Harris parameters $\mathcal{J}_0 = 35\hbar^2\,\mathrm{MeV}^{-1}$ and $\mathcal{J}_1 = 40\hbar^4\,\mathrm{MeV}^{-3}$.

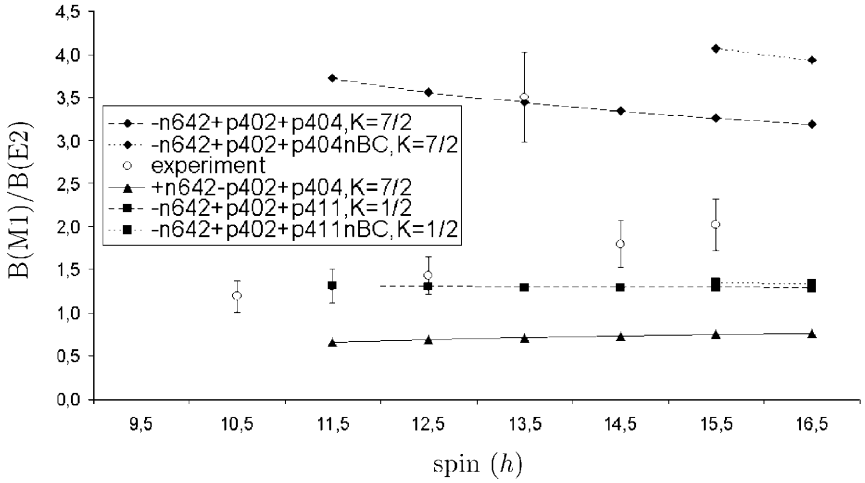

Fig. 9. Experimental and calculated $B(M1)/B(E2)$ ratios as a function of spin for the bands ka,kb. The bump at $I = 13.5\hbar$ in the set of experimental points is due to a very weak $E2$ transition at 406 keV.

4.4 The bands Ka,Kb and ka,kb

It has not been determined if the lowest observed states of the pairs of bands, k and K, are the true bandheads, which would imply $K^\pi = 21/2^-$ for bands Ka and Kb and $K^\pi = 15/2^+$ for bands ka and kb. The total observed intensity of the decay transitions of both pairs of bands, K and k, match the population of the bands, meaning there is no substantial loss in intensity due to a rise in lifetime for the lowest states. With a velocity ratio of $v/c \approx 4\%$, the compound nucleus travels at ~ 1.2 cm/ns, implying an upper limit of 10 ns for the lifetime of the lowest levels, in order for the deexciting gamma rays to reach the detectors. Should the lowest observed levels be the true bandheads, the decay transitions from the two pairs of bands, K and k, would have $\Delta K = 8$ and 5, respectively, and the K-forbidden decay transitions should have resulted in a longer lifetime for the states. Thus, either the lowest observed states are not the true bandheads, or, if they were, the K-quantum number is strongly mixed.

Based on observed alignments, high excitation energy and strong $M1$ transitions, it is our judgement that the pairs of bands, K and k, both are associated with three-quasiparticle configurations consisting of one neutron and a proton pair. The proton orbitals closest to the Fermi level are listed in table 3 together with their associated experimental alignments and calculated values of g_K. For the calculations of $B(M1)$-values of the possible configurations the extension of the geometrical model of ref. [15] has been used with the g_K-values for the protons listed in table 3, a value of $g_K = -0.28$ for the only relevant neutron orbital, $i_{13/2}[642]5/2^+$, and a collective gyromagnetic ratio $g_R = 0.35$.

The bands ka and kb follow band A on an alignment plot, see fig. 8, experiencing a late crossing around 315 keV, interpreted as a BC crossing. The missing AB crossing is understood as a blocking phenomenon and, consequently, the A neutron orbital must be contained in the configuration of these bands. As may be noted from the alignment plot, the coupled protons of the configuration do not contribute to the alignment of bands ka and kb, a fact that rules out the $[541]1/2^-$ orbital, and subsequently the $[514]9/2^-$ orbital as well, as this is the only remaining orbital with negative parity and the coupled protons must contribute with positive parity. Numerous $B(M1)/B(E2)$ calculations have not singled out any clear candidate for the configuration, although the plots of fig. 9, slightly favour the configuration $\nu[642]5/2^+ \otimes [\pi[402]5/2^+ \otimes \pi[411]1/2^+]_{K=3}$, coupled to $K^\pi = 1/2^+$. This configuration assignment should only be considered as a suggestion. It implies that the decay-out is not K-hindered and occurs above the bandhead, in competition with the (unseen) in-band $E2$ and $M1$ transitions for which lifetimes are estimated to be several tens of ps. The structural change associated with the decay of band kb to bands A, B and E would imply the annihilation of the two-quasiproton excitation, and in the case of decay to band E, also the presence of sizeable $E1$ transition strength connecting the $[642]5/2^+$ and $[523]5/2^-$ orbitals. Strong $E1$ matrix elements are indeed found in the decays from band F to band A and from band E to band B in this nucleus, see fig. 1.

For the bands Ka and Kb a choice of a high K-value of $K = 21/2$ causes the bands to display an AB crossing, while a BC crossing is seen for a choice of a low K-value. The latter scenario is preferred and, as before, we conclude that the configuration of bands Ka and Kb contains the A neutron. The full configuration proposed is $\nu[642]5/2^+ \otimes [\pi[514]9/2^- \otimes \pi[411]1/2^+]_{K=5}$, coupled to $K^\pi = 15/2^-$, for which the calculated $B(M1)/B(E2)$ ratios agree with the data. Hence, the intense $E1$ decay occurs before the bandhead is populated, allowing a restriction on the lifetime of the lowest levels of the K bands. By estimating the transition rates of the next (unseen) in-band $E2$ and $M1$ transitions from the $21/2^-$ level, we assess the lifetime of this level to be on the order of 10 ps. Thus, the decay out has $\Delta K = 5$, which makes the transition four times K-forbidden. The aligned A orbital is,

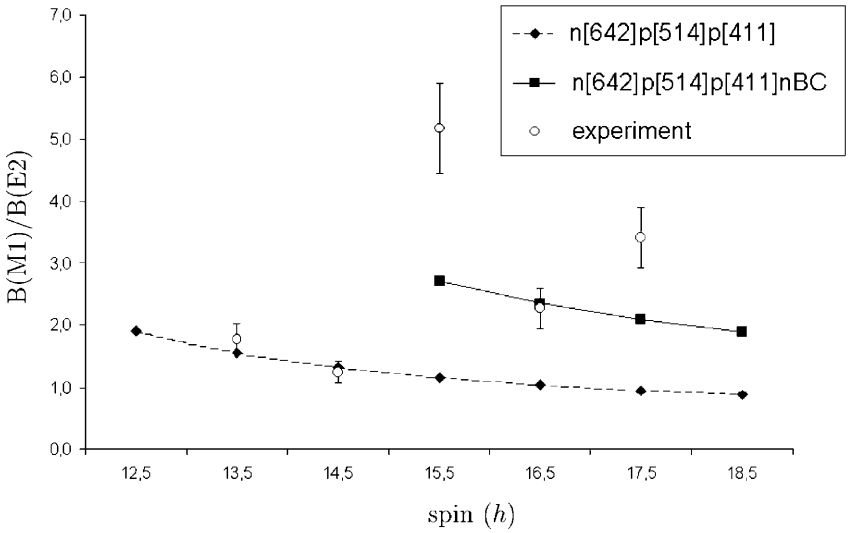

Fig. 10. Experimental $B(M1)/B(E2)$ ratios compared to theoretical calculations for the proposed configuration of the bands Ka,Kb, with and without an aligned (BC) neutron pair.

therefore, assumed to introduce a wide K-distribution. The introduction of the $\pi[411]1/2^+$ orbital is justified by its presence [10] in the lutetium ground states and, in particular, by its identification in ^{169}Lu. Furthermore, the orbital is low-lying in the UC calculations.

It is interesting to note that these two pairs of strongly coupled bands in ^{169}Hf are different regarding $B(M1)/B(E2)$-values from the two pairs observed recently in ^{171}Hf which have been assigned [16] as high-K couplings of the $i_{13/2}$ neutron to the proton configurations $[514]9/2^- \otimes [404]7/2^+$ and $[402]5/2^+ \otimes [404]7/2^+$ with $K^\pi = 23/2^-$ and $19/2^+$, respectively. Furthermore, the excitation energies of the bands Ka,Kb and ka,kb relative to band A are higher than the corresponding relative excitation energy of the high-K bands in ^{171}Hf by several hundred keV.

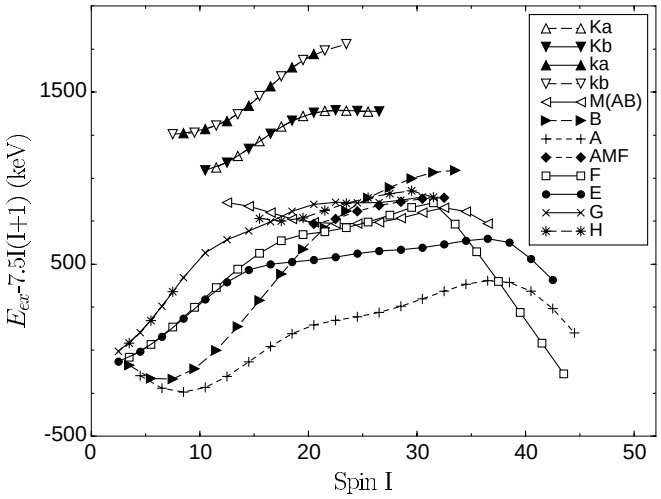

Fig. 11. Excitation energy with a rigid rotor reference subtracted, as a function of spin, for all bands in the level scheme.

4.5 High-spin proton alignment

The energy *vs.* spin plot of fig. 11 displays a very similar downslope at high spins for the bands reaching sufficient angular momentum, indicating the intrusion of new down sloping configurations becoming energetically favourable in this domain. All four bands developed into the high-spin region display an upbend on the alignment plot (fig. 12) at high frequency corresponding to a second bandcrossing. These frequencies have been determined to lie in the range 450 keV $< \hbar\omega <$ 565 keV (table 4).

For bands A, E and M the full alignment cannot be ascertained as they have not been observed at sufficiently high spins. However, the alignment gain will exceed three and a half units in all cases, meaning that the bands have five quasiparticle configurations above the mentioned frequencies. Previous CSM calculations have been performed for ^{169}Hf by Gao *et al.* [6], which predict second band crossings due to the second $i_{13/2}$ neutron crossing, an $h_{11/2}$ proton pair, an $h_{9/2}$ proton pair and finally a mixture of $h_{9/2}$ and $h_{11/2}$ proton orbitals. Our Ultimate Cranker calculations predict the same ordering of the band crossings as ref. [6] (see table 5), but at somewhat lower frequencies, an effect caused by the use of a slightly larger deformation. In ref. [6] a moderate decrease of the quadrupole moments with increasing frequency has been experimentally observed. The possibility of lower deformation at higher spins may explain the difference between the observed crossing frequencies and our calculations. The calculated crossing frequencies of table 5 are highly deformation dependent.

The CD crossing is blocked for band A(BC) and, thus, the second upbend of this band must be explained by the alignment of a proton pair. The $\pi h_{11/2}$ pair is ruled out as the observed crossing frequencies lie above the predicted critical frequency of the $\pi h_{11/2}$ pair and the alignment gain from such a pair is too small. This leaves two possibilities, either a $\pi h_{9/2}$ pair or a mixture of the $h_{9/2}$

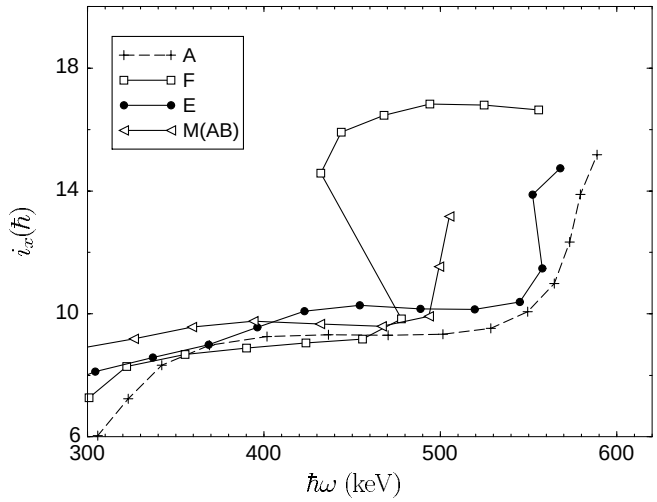

Fig. 12. Alignment of the bands reaching the highest spins relative to a reference with Harris parameters $\mathcal{J}_0 = 35\hbar^2\,\mathrm{MeV}^{-1}$ and $\mathcal{J}_1 = 40\hbar^4\,\mathrm{MeV}^{-3}$. The experimental crossing frequencies for the second crossing and the subsequent alignment gains are given in table 4.

Table 4. Crossing frequencies and alignment gains at high spin.

Band	Crossing frequency	Alignment gain
F(AB)	≈ 450 keV	$\approx 6.5\hbar$
M(AB)	≈ 490 keV	$> 3.5\hbar$
E(AB)	≈ 550 keV	$> 4.0\hbar$
A(BC)	≈ 565 keV	$> 5.0\hbar$

and $h_{11/2}$ proton orbitals. We would like to emphasize that the latter is the configuration calculated to exhibit a crossing with sufficient alignment at the lowest frequency. At high frequencies such as these, the $\alpha = +1/2$ components of $\pi h_{11/2}$ and $\pi h_{9/2}$ orbitals are reversed and a "mixed" crossing may account for the observed effect. Mixed crossings such as this one have also been discussed in the osmium-iridium region [17], but more appropriately, this effect has previously been proposed for ^{169}Hf [6], ^{167}Hf [11] and, very recently, for ^{166}Hf [18]. The proposed Nilsson configuration of the proton pair responsible for the second upbend is $\pi[541]1/2^-(\alpha = +1/2) \otimes \pi[514]9/2^-(\alpha = -1/2)$. Should this configuration be responsible for the upbend in all four bands, the dispersion in crossing frequencies could possibly be explained by the fact that these crossing frequencies are sensitive to deformation changes since the $[541]1/2^-$ orbital shows a particularly strong deformation dependence. The 100 keV difference in crossing frequency for bands E(AB) and F(AB) may indicate a signature dependence on deformation. Alternatively, one might consider the configuration $\pi[404]7/2^+(\alpha = -1/2) \otimes \pi[660]1/2^+(\alpha = +1/2)$. The UC calculations show that the alignment of this pair may occur at frequencies similar to that of the mixed crossing of the $\pi h_{11/2}$ and $\pi h_{9/2}$ orbitals. The pronounced decline of the $\pi[660]1/2^+$ orbital as a function of rotational frequency is well known, and this orbital alone is expected to contribute about $4\hbar$ to the alignment.

Table 5. Calculated crossing frequencies and alignment gain.

Aligning quasiparticles	Crossing frequency	Alignment gain
$\pi h_{11/2}$	420 keV	~ 2
$\pi h_{11/2} h_{9/2}$	450 keV	~ 5
$\pi i_{13/2} g_{7/2}$	505 keV	~ 5
$\pi h_{9/2}$	540 keV	~ 5.5
$\nu i_{13/2}$ (CD)	620 keV	~ 3.5

5 Summary

The present study of the even-odd nucleus, ^{169}Hf, has resulted in a substantial extension of the six previously known rotational bands and the discovery of six new bands. Spin and parities of the new bands have been determined by considering the DCO ratios as well as the relative populations. To three of the new bands positive parity has been assigned, the remaining three bands have negative parity. Of the six new bands, four form coupled pairs connected by strong $M1$ transitions. Both coupled pairs of bands are believed to contain two quasiprotons in their three-quasiparticle configurations. Two such configurations have been proposed, but, as noted, there are considerable uncertainties associated with these assignments.

The new band decaying into the B band, before reaching the lowest levels, is assigned to the M quasineutron based on the $[521]1/2^-$ orbital. This conclusion was reached after comparison to the Ultimate Cranker calculations and the systematics of the numerous nuclei in the region containing the M quasineutron. The band is observed after the AB crossing and thus has a three quasiparticle configuration, M(AB), in the mid-spin region. For yet higher spins a substantial increase in alignment is observed, caused by the alignment of a second quasiparticle pair. There are several indications of a mixing between the last new band, the AMF band, and a γ-vibrational state. These include enhanced branching ratios, five connecting $E2$ transitions ($\Delta I = 2$) with unusually high energy and two connecting $E2$ transitions ($\Delta I = 0$) with energies comparable to similar transitions between γ-vibrational bands and the ground bands in neighbouring even-even hafnium nuclei. The assigned configuration, therefore, naturally consists of a two-quasiparticle configuration coupled to $K = 2$, in unison with the A quasineutron orbital.

Four bands were extended to such high spins that a second clear upbend was observed. We conclude that these bands are associated with five quasiparticle configurations at the highest spins and, furthermore, that the aligning orbital pair is a proton pair. The alignment of a mixture of the $h_{9/2}$ and $h_{11/2}$ proton orbitals is the most likely explanation for the observed upbend. Future studies of this nucleus should reach even higher spins and seek to clarify the mechanism(s) responsible for this second band crossing.

This work is supported by the Danish Natural Research Foundation, BMBF (Germany) under contract no. 06BN907, the U.S. Department of Energy, Nuclear Science Division under contract no. W-31-109-ENG38 and the Polish Committee for Scientific Research (KBN grant no. 2 P03 B001 16).

Appendix A.

Table 6. Energies of levels and γ-rays added to the level scheme of [6] from the present experiment. Level energy errors average 1–2 keV for the highest excitations. Transition energies have errors on the order of 0.2–0.4 keV. Intensities are for each band estimated from low double gates. They have been corrected to correspond to branching ratios determined from gates above, in cases where such branchings are analysed.

E_i	$\mathrm{Band_i}$	$\rightarrow$	$\mathrm{Band_f}$	J^π_i	$\rightarrow$	J^π_f	E_γ	I_γ
9568	A	$\rightarrow$	A	$69/2^+$	$\rightarrow$	$65/2^+$	1059.2	5.8(7)
10669	A	$\rightarrow$	A	$73/2^+$	$\rightarrow$	$69/2^+$	1100.8	3.1(7)
11800	A	$\rightarrow$	A	$77/2^+$	$\rightarrow$	$73/2^+$	1130.7	1.6(7)
12948	A	$\rightarrow$	A	$81/2^+$	$\rightarrow$	$77/2^+$	1148.2	1.1(6)
14108	A	$\rightarrow$	A	$85/2^+$	$\rightarrow$	$81/2^+$	1160.1	0.7(6)
15287	A	$\rightarrow$	A	$89/2^+$	$\rightarrow$	$85/2^+$	1178.8	< 0.5
5953	B	$\rightarrow$	B	$51/2^+$	$\rightarrow$	$47/2^+$	825.1	4.5(5)
6824	B	$\rightarrow$	B	$55/2^+$	$\rightarrow$	$51/2^+$	871.8	3.5(5)
7746	B	$\rightarrow$	B	$59/2^+$	$\rightarrow$	$55/2^+$	921.4	1.3(5)
8712	B	$\rightarrow$	B	$63/2^+$	$\rightarrow$	$59/2^+$	966.1	0.4(4)
9713	B	$\rightarrow$	B	$67/2^+$	$\rightarrow$	$63/2^+$	1001.6	< 0.3
8780	E	$\rightarrow$	E	$65/2^-$	$\rightarrow$	$61/2^-$	978.5	4.0(5)
9820	E	$\rightarrow$	E	$69/2^-$	$\rightarrow$	$65/2^-$	1040.8	2.6(5)
10912	E	$\rightarrow$	E	$73/2^-$	$\rightarrow$	$69/2^-$	1091.9	1.4(4)
12030	E	$\rightarrow$	E	$77/2^-$	$\rightarrow$	$73/2^-$	1117.3	0.8(4)
13136	E	$\rightarrow$	E	$81/2^-$	$\rightarrow$	$77/2^-$	1106	1.0(4)
14273	E	$\rightarrow$	E	$85/2^-$	$\rightarrow$	$81/2^-$	1137	< 0.5
5813	F	$\rightarrow$	F	$51/2^-$	$\rightarrow$	$47/2^-$	782.8	7.0(3)
6663	F	$\rightarrow$	F	$55/2^-$	$\rightarrow$	$51/2^-$	850.0	4.8(4)
7577	F	$\rightarrow$	F	$59/2^-$	$\rightarrow$	$55/2^-$	914.0	3.1(3)
8535	F	$\rightarrow$	F	$63/2^-$	$\rightarrow$	$59/2^-$	958.0	2.0(3)
9401	F	$\rightarrow$	F	$67/2^-$	$\rightarrow$	$63/2^-$	866.1	1.2(4)
10290	F	$\rightarrow$	F	$71/2^-$	$\rightarrow$	$67/2^-$	889.3	1.4(4)
11228	F	$\rightarrow$	F	$75/2^-$	$\rightarrow$	$71/2^-$	937.4	1.0(3)
12217	F	$\rightarrow$	F	$79/2^-$	$\rightarrow$	$75/2^-$	989.4	1.3(5)
13268	F	$\rightarrow$	F	$83/2^-$	$\rightarrow$	$79/2^-$	1051.0	1.0(3)
14381	F	$\rightarrow$	F	$87/2^-$	$\rightarrow$	$83/2^-$	1112.7	0.8(3)
1027	G	$\rightarrow$	G	$17/2^-$	$\rightarrow$	$13/2^-$	406.2	1.0(3)
1471	G	$\rightarrow$	G	$21/2^-$	$\rightarrow$	$17/2^-$	443.9	1.0(3)
1907	G	$\rightarrow$	G	$25/2^-$	$\rightarrow$	$21/2^-$	436.0	0.9(3)
1907	G	$\rightarrow$	E	$25/2^-$	$\rightarrow$	$21/2^-$	707.0	0.5(2)
2379	G	$\rightarrow$	G	$29/2^-$	$\rightarrow$	$25/2^-$	471.4	1.2(3)
2379	G	$\rightarrow$	E	$29/2^-$	$\rightarrow$	$25/2^-$	718.0	0.8(3)
2912	G	$\rightarrow$	G	$33/2^-$	$\rightarrow$	$29/2^-$	533.6	2.0(4)
2912	G	$\rightarrow$	E	$33/2^-$	$\rightarrow$	$29/2^-$	760.5	0.9(3)
3513	G	$\rightarrow$	G	$37/2^-$	$\rightarrow$	$33/2^-$	600.4	2.7(3)
3513	G	$\rightarrow$	E	$37/2^-$	$\rightarrow$	$33/2^-$	847.8	0.7(3)
4154	G	$\rightarrow$	G	$41/2^-$	$\rightarrow$	$37/2^-$	640.9	2.9(5)
4154	G	$\rightarrow$	E	$41/2^-$	$\rightarrow$	$37/2^-$	935.4	0.7(3)
4825	G	$\rightarrow$	G	$45/2^-$	$\rightarrow$	$41/2^-$	671.7	3.6(6)
5542	G	$\rightarrow$	G	$49/2^-$	$\rightarrow$	$45/2^-$	716.8	2.8(6)
6324	G	$\rightarrow$	G	$53/2^-$	$\rightarrow$	$49/2^-$	781.9	2.1(4)
7178	G	$\rightarrow$	G	$57/2^-$	$\rightarrow$	$53/2^-$	853.5	1.6(6)
8097	G	$\rightarrow$	G	$61/2^-$	$\rightarrow$	$57/2^-$	919.3	1.0(4)
2683	H	$\rightarrow$	A	$31/2^-$	$\rightarrow$	$29/2^+$	1065.2	0.7(3)
3179	H	$\rightarrow$	H	$35/2^-$	$\rightarrow$	$31/2^-$	495.5	0.8(3)
3179	H	$\rightarrow$	A	$35/2^-$	$\rightarrow$	$33/2^+$	992.0	0.7(3)
3767	H	$\rightarrow$	H	$39/2^-$	$\rightarrow$	$35/2^-$	588.3	1.3(3)
3767	H	$\rightarrow$	F	$39/2^-$	$\rightarrow$	$35/2^-$	703.1	0.8(3)
3767	H	$\rightarrow$	A	$39/2^-$	$\rightarrow$	$37/2^+$	964.9	1.4(4)
4440	H	$\rightarrow$	H	$43/2^-$	$\rightarrow$	$39/2^-$	673.0	2.8(5)

Table 6. (*Continued*).

E_i	$\mathrm{Band_i}$	$\rightarrow$	$\mathrm{Band_f}$	J_i^π	$\rightarrow$	J_f^π	E_γ	I_γ
4440	H	$\rightarrow$	A	$43/2^-$	$\rightarrow$	$41/2^+$	988.4	0.8(3)
5172	H	$\rightarrow$	H	$47/2^-$	$\rightarrow$	$43/2^-$	732.0	3.3(5)
5172	H	$\rightarrow$	A	$47/2^-$	$\rightarrow$	$45/2^+$	1033.2	0.8(3)
5954	H	$\rightarrow$	H	$51/2^-$	$\rightarrow$	$47/2^-$	782.0	4.0(5)
6788	H	$\rightarrow$	H	$55/2^-$	$\rightarrow$	$51/2^-$	834.0	2.3(4)
7675	H	$\rightarrow$	H	$59/2^-$	$\rightarrow$	$55/2^-$	887.0	1.6(6)
8567	H	$\rightarrow$	H	$63/2^-$	$\rightarrow$	$59/2^-$	891.8	0.6(3)
2125	M(AB)	$\rightarrow$	B	$25/2^-$	$\rightarrow$	$23/2^+$	1047.1	1.5(5)
2523	M(AB)	$\rightarrow$	M(AB)	$29/2^-$	$\rightarrow$	$25/2^-$	398.0	1.5(5)
2523	M(AB)	$\rightarrow$	B	$29/2^-$	$\rightarrow$	$27/2^+$	917.3	4.5(5)
2967	M(AB)	$\rightarrow$	M(AB)	$33/2^-$	$\rightarrow$	$29/2^-$	443.9	6.0(6)
2967	M(AB)	$\rightarrow$	B	$33/2^-$	$\rightarrow$	$31/2^+$	758.8	3.2(3)
3469	M(AB)	$\rightarrow$	M(AB)	$37/2^-$	$\rightarrow$	$33/2^-$	502.2	9.2(5)
4051	M(AB)	$\rightarrow$	M(AB)	$41/2^-$	$\rightarrow$	$37/2^-$	581.7	8.2(7)
4703	M(AB)	$\rightarrow$	M(AB)	$45/2^-$	$\rightarrow$	$41/2^-$	652.7	6.6(7)
5422	M(AB)	$\rightarrow$	M(AB)	$49/2^-$	$\rightarrow$	$45/2^-$	718.6	4.2(5)
6210	M(AB)	$\rightarrow$	M(AB)	$53/2^-$	$\rightarrow$	$49/2^-$	788.1	3.5(6)
7074	M(AB)	$\rightarrow$	M(AB)	$57/2^-$	$\rightarrow$	$53/2^-$	863.6	2.3(6)
8007	M(AB)	$\rightarrow$	M(AB)	$61/2^-$	$\rightarrow$	$57/2^-$	933.5	1.2(4)
8994	M(AB)	$\rightarrow$	M(AB)	$65/2^-$	$\rightarrow$	$61/2^-$	987.0	1.1(4)
9993	M(AB)	$\rightarrow$	M(AB)	$69/2^-$	$\rightarrow$	$65/2^-$	998.7	0.8(4)
11003	M(AB)	$\rightarrow$	M(AB)	$73/2^-$	$\rightarrow$	$69/2^-$	1010.1	0.7(4)
4040	AMF	$\rightarrow$	A	$41/2^+$	$\rightarrow$	$41/2^+$	587.9	< 0.3
4040	AMF	$\rightarrow$	A	$41/2^+$	$\rightarrow$	$37/2^+$	1237.4	0.6(2)
4728	AMF	$\rightarrow$	A	$45/2^+$	$\rightarrow$	$45/2^+$	588.9	< 0.3
4728	AMF	$\rightarrow$	AMF	$45/2^+$	$\rightarrow$	$41/2^+$	688.2	0.8(3)
4728	AMF	$\rightarrow$	A	$45/2^+$	$\rightarrow$	$41/2^+$	1276.2	0.6(2)
5494	AMF	$\rightarrow$	AMF	$49/2^+$	$\rightarrow$	$45/2^+$	765.7	1.3(4)
5494	AMF	$\rightarrow$	A	$49/2^+$	$\rightarrow$	$45/2^+$	1354.6	0.9(3)
6307	AMF	$\rightarrow$	AMF	$53/2^+$	$\rightarrow$	$49/2^+$	813.3	2.1(5)
6307	AMF	$\rightarrow$	A	$53/2^+$	$\rightarrow$	$49/2^+$	1427.1	0.8(3)
7168	AMF	$\rightarrow$	AMF	$57/2^+$	$\rightarrow$	$53/2^+$	860.9	2.5(5)
7168	AMF	$\rightarrow$	A	$57/2^+$	$\rightarrow$	$53/2^+$	1482.1	< 0.5
8086	AMF	$\rightarrow$	AMF	$61/2^+$	$\rightarrow$	$57/2^+$	918.1	1.8(4)
9051	AMF	$\rightarrow$	AMF	$65/2^+$	$\rightarrow$	$61/2^+$	965.4	0.9(4)
1866	ka	$\rightarrow$	kb	$17/2^+$	$\rightarrow$	$15/2^+$	132.9	0.7(2)
2191	ka	$\rightarrow$	kb	$21/2^+$	$\rightarrow$	$19/2^+$	178.8	1.6(2)
2191	ka	$\rightarrow$	ka	$21/2^+$	$\rightarrow$	$17/2^+$	324.4	0.5(1)
2597	ka	$\rightarrow$	kb	$25/2^+$	$\rightarrow$	$23/2^+$	213.5	1.8(2)
2597	ka	$\rightarrow$	ka	$25/2^+$	$\rightarrow$	$21/2^+$	406.2	0.4(1)
3107	ka	$\rightarrow$	kb	$29/2^+$	$\rightarrow$	$27/2^+$	266.7	1.8(2)
3107	ka	$\rightarrow$	ka	$29/2^+$	$\rightarrow$	$25/2^+$	509.5	1.1(2)
3699	ka	$\rightarrow$	kb	$33/2^+$	$\rightarrow$	$31/2^+$	304.5	1.4(2)
3699	ka	$\rightarrow$	ka	$33/2^+$	$\rightarrow$	$29/2^+$	592.8	1.2(2)
4350	ka	$\rightarrow$	kb	$37/2^+$	$\rightarrow$	$35/2^+$	330.2	1.4(3)
4350	ka	$\rightarrow$	ka	$37/2^+$	$\rightarrow$	$33/2^+$	650.3	1.2(2)
5027	ka	$\rightarrow$	kb	$41/2^+$	$\rightarrow$	$39/2^+$	342.0	0.7(2)
5027	ka	$\rightarrow$	ka	$41/2^+$	$\rightarrow$	$37/2^+$	676.9	0.5(2)
1734	kb	$\rightarrow$	B	$15/2^+$	$\rightarrow$	$19/2^+$	1092.8	0.9(2)
1734	kb	$\rightarrow$	E	$15/2^+$	$\rightarrow$	$13/2^-$	1290.1	0.5(1)
1734	kb	$\rightarrow$	A	$15/2^+$	$\rightarrow$	$17/2^+$	1370.5	~ 0.1
1734	kb	$\rightarrow$	B	$15/2^+$	$\rightarrow$	$15/2^+$	1423.0	1.1(2)
2012	kb	$\rightarrow$	ka	$19/2^+$	$\rightarrow$	$17/2^+$	145.6	0.9(2)
2012	kb	$\rightarrow$	kb	$19/2^+$	$\rightarrow$	$15/2^+$	278.5	1.0(2)
2384	kb	$\rightarrow$	ka	$23/2^+$	$\rightarrow$	$21/2^+$	192.7	1.1(2)
2384	kb	$\rightarrow$	kb	$23/2^+$	$\rightarrow$	$19/2^+$	371.5	0.5(1)

Table 6. (*Continued*)

E_i	Band_i	→	Band_f	J_i^π	→	J_f^π	E_γ	I_γ
2840	kb	→	ka	$27/2^+$	→	$25/2^+$	242.8	2.0(1)
2840	kb	→	kb	$27/2^+$	→	$23/2^+$	456.3	1.1(1)
3395	kb	→	ka	$31/2^+$	→	$29/2^+$	288.3	1.5(1)
3395	kb	→	kb	$31/2^+$	→	$27/2^+$	555.1	1.0(3)
4020	kb	→	ka	$35/2^+$	→	$33/2^+$	320.2	1.3(1)
4020	kb	→	kb	$35/2^+$	→	$31/2^+$	624.6	1.0(3)
4685	kb	→	ka	$39/2^+$	→	$37/2^+$	334.9	1.0(1)
4685	kb	→	kb	$39/2^+$	→	$35/2^+$	665.1	0.8(3)
5371	kb	→	ka	$43/2^+$	→	$41/2^+$	343.9	0.6(2)
5371	kb	→	kb	$43/2^+$	→	$39/2^+$	685.9	0.5(2)
6097	kb	→	kb	$47/2^+$	→	$43/2^+$	726.6	0.5(2)
2140	Ka	→	Kb	$23/2^-$	→	$21/2^-$	187.9	2.7(2)
2596	Ka	→	Kb	$27/2^-$	→	$25/2^-$	240.0	2.7(2)
2596	Ka	→	Ka	$27/2^-$	→	$23/2^-$	456.6	2.2(2)
3133	Ka	→	Kb	$31/2^-$	→	$29/2^-$	277.2	2.0(2)
3133	Ka	→	Ka	$31/2^-$	→	$27/2^-$	536.7	1.3(2)
3727	Ka	→	Kb	$35/2^-$	→	$33/2^-$	303.7	1.7(2)
3727	Ka	→	Ka	$35/2^-$	→	$31/2^-$	594.5	1.3(2)
4360	Ka	→	Kb	$39/2^-$	→	$37/2^-$	319.6	1.2(2)
4360	Ka	→	Ka	$39/2^-$	→	$35/2^-$	632.2	1.1(2)
5019	Ka	→	Kb	$43/2^-$	→	$41/2^-$	332.9	1.5(2)
5019	Ka	→	Ka	$43/2^-$	→	$39/2^-$	659.9	1.4(3)
5710	Ka	→	Kb	$47/2^-$	→	$45/2^-$	350.0	0.9(2)
5710	Ka	→	Ka	$47/2^-$	→	$43/2^-$	690.7	0.8(2)
6454	Ka	→	Kb	$51/2^-$	→	$49/2^-$	377.9	0.6(2)
6454	Ka	→	Ka	$51/2^-$	→	$47/2^-$	743.7	0.5(2)
1952	Kb	→	*B*	$21/2^-$	→	$23/2^+$	873.6	4.7(5)
1952	Kb	→	*B*	$21/2^-$	→	$19/2^+$	1310.9	0.9(3)
2356	Kb	→	Ka	$25/2^-$	→	$23/2^-$	216.6	3.1(2)
2356	Kb	→	Kb	$25/2^-$	→	$21/2^-$	404.5	1.3(2)
2856	Kb	→	Ka	$29/2^-$	→	$27/2^-$	259.5	2.2(2)
2856	Kb	→	Kb	$29/2^-$	→	$25/2^-$	499.5	0.6(2)
3424	Kb	→	Ka	$33/2^-$	→	$31/2^-$	290.8	1.7(2)
3424	Kb	→	Kb	$33/2^-$	→	$29/2^-$	568.0	0.8(2)
4040	Kb	→	Ka	$37/2^-$	→	$35/2^-$	312.6	1.7(2)
4040	Kb	→	Kb	$37/2^-$	→	$33/2^-$	616.3	1.3(2)
4687	Kb	→	Ka	$41/2^-$	→	$39/2^-$	327.0	1.9(4)
4687	Kb	→	Kb	$41/2^-$	→	$37/2^-$	646.6	1.7(4)
5360	Kb	→	Ka	$45/2^-$	→	$43/2^-$	340.7	0.9(3)
5360	Kb	→	Kb	$45/2^-$	→	$41/2^-$	673.6	0.9(3)
6076	Kb	→	Ka	$49/2^-$	→	$47/2^-$	365.8	0.8(3)
6076	Kb	→	Kb	$49/2^-$	→	$45/2^-$	715.8	0.9(3)
6853	Kb	→	Ka	$53/2^-$	→	$51/2^-$	398.9	0.4(2)
6853	Kb	→	Kb	$53/2^-$	→	$49/2^-$	776.8	0.5(2)

References

1. T. Bengtsson, Nucl. Phys. A **496**, 56 (1989); **512**, 124 (1990).
2. See `http://www.matfys.lth.se/~ragnar/ultimate.html`.
3. I-Y. Lee, Nucl. Phys. A **520**, 641 (1990).
4. J. Eberth et al., Nucl. Instrum. Methods A **369**, 135 (1996).
5. H. Amro et al., Phys. Lett. B **506**, 39 (2001).
6. W.B. Gao, I.Y. Lee, C. Baktash, R. Wyss, J.H. Hamilton, C.M. Steele, C.H. Yu, N.R. Johnson, F.K. McGowan, Phys. Rev. C **44**, 1380 (1991).
7. D.C. Radford, Nucl. Instrum. Methods A **361**, 297 (1995).
8. M. Bergström, Plotwidgets Ref. Man., NBI internal report (1999).
9. I. Rezanka, I.M. Ladenbauer-Bellis, J.O. Rasmussen, W. Ribbe, E. der Mateosian, Phys. Rev. C **11**, 1767 (1975).
10. R.B. Firestone et al. *Table of Isotopes*, Vol. **II** (John Wiley & Sons, 1996).
11. M.B. Smith, G.J. Campbell, R. Chapman, P.O. Tjøm, R.A. Bark, G.B. Hagemann, N. Keeley, D.J. Middleton, H. Ryde, K.-M. Spoh, Eur. Phys. J. A **6**, 37 (1999).
12. G.B. Hagemann, H. Ryde, P. Bosetti, A. Brockstedt, H. Carlsson, L.P. Ekström, A. Nordlund, R.A. Bark, B. Her-

skind, S. Leoni, A. Bracco, F. Camera, S. Frattini, M. Mattiuzzi, B. Million, C. Rossi-Avarez, G. de Angelis, D. Bazzacco, S. Lunardi, M. de Poli, Nucl. Phys. A **618**, 199 (1997).
13. R. Bengtsson, S. Frauendorf, F.R. May, At. Data Nucl. Data Tables **35**, 15 (1986).
14. H.J. Jensen, R.A. Bark, R. Bengtsson, G.B. Hagemann, P.O. Tjøm, S.Y. Araddad, C.W. Beausang, R. Chapman, J. Copnell, A. Fitzpatrick, S.J. Freeman, S. Leoni, J.C. Lisle, J. Simpson, A.G. Smith, D.M. Tompson, S.J. Warburton, J. Wrzesinski, Z. Phys. A **359**, 127 (1997).
15. F. Dönau, Nucl. Phys. A **471**, 469 (1987).
16. D.M. Cullen, D.E. Appelbe, A.T. Reed, C. Baktash, C.-H. Yu, Phys. Rev. C **55**, 508 (1997).
17. E.R. Marshalek, R. Blömel, Phys. Rev. Lett. **55**, 370 (1985).
18. D. Ringkjøbing Jensen, J. Domscheit, G.B. Hagemann, M. Bergström, B. Herskind, B.S. Nielsen, G. Sletten, P.G. Varmette, S. Törmänen, H. Hübel, W.C. Ma, A. Bracco, F. Camera, F. Demaria, S. Frattini, B. Million, D. Napoli, A. Maj, B.M. Nyako, D.T. Joss, M. Aiche, Eur. Phys J. A **8**, 165 (2000).